

Low-temperature transport, thermal, and optical properties of single-grain quasicrystals of icosahedral phases in the Y-Mg-Zn and Tb-Mg-Zn alloy systems

M. A. Chernikov,* S. Paschen,[†] E. Felder, P. Vorburger, B. Ruzicka, L. Degiorgi, and H. R. Ott
Laboratorium für Festkörperphysik, Eidgenössische Technische Hochschule-Zürich, 8093 Zürich, Switzerland

I. R. Fisher and P. C. Canfield

Ames Laboratory and Department of Physics and Astronomy, Iowa State University, Ames, Iowa 50011

(Received 17 November 1999)

We present a comprehensive series of results of electrical transport (electrical conductivity, magnetoconductivity, Hall effect), thermal (specific heat), and optical (reflectivity) measurements in varying temperature ranges between 1.5 and 300 K on high-quality single-grain quasicrystals of icosahedral Y-Mg-Zn. This data set is augmented by the specific-heat and optical-reflectivity data obtained from a single-grain quasicrystal of icosahedral Tb-Mg-Zn. For Y-Mg-Zn, both the electrical conductivity $\sigma(T)$ and magnetoconductivity $\delta\sigma(H)$ may be described by calculations considering quantum interference effects. A detailed comparison of the weak-localization contributions to $\sigma(T)$ and $\delta\sigma(H)$ with our experimental data provides estimates of the inelastic and spin-orbit relaxation rates. The inelastic relaxation rate is found to be proportional to T^3 . The dominant contributions to the optical conductivity $\sigma_1(\omega)$ spectrum, obtained from the reflectivity $R(\omega)$ data in the frequency range between 16 and 9.7×10^4 cm^{-1} , are a strong Drude feature at low frequencies and a prominent absorption signal centered at approximately 6×10^3 cm^{-1} . A comparison of the spectral weight of the Drude contribution to $\sigma_1(\omega)$ with the magnitude of the linear-in- T term γT of the low-temperature specific heat $C_p(T)$ yields the itinerant charge-carrier density $n_i = 7.62 \times 10^{21}$ cm^{-3} or 0.13 charge carriers per atom. The low n_i value is corroborated by the results of the Hall effect measurements. For Tb-Mg-Zn, the optical conductivity $\sigma_1(\omega)$ spectrum reveals features similar to those of Y-Mg-Zn. The low-temperature specific heat $C_p(T)$ of Tb-Mg-Zn is strongly influenced by a spin-glass-type freezing of Tb moments and by crystal-electric-field effects.

I. INTRODUCTION

A thermodynamically stable icosahedral phase in the Y-Mg-Zn alloy system was identified by Luo and co-workers.¹ Its powder x-ray-diffraction pattern turned out to be identical with the Y-Mg-Zn Z-phase found more than a decade earlier by Padezhnova and co-workers.² Subsequent investigations have shown that thermally stable icosahedral phases also form when Y is fully substituted by Tb, Dy, Ho or Er.^{3,4} These are, so far, the only stable phases that allow the study of the features of localized $4f$ magnetic moments arranged on an icosahedrally ordered quasiperiodic lattice.

Icosahedral quasicrystals in the R -Mg-Zn ($R = \text{Y, Tb, Dy, Ho or Er}$) ternary systems crystallize in a face-centered-icosahedral (fci) structure of the Frank-Kasper type. This sets them apart from Al-based thermodynamically stable fci phases, which crystallize in a Mackay-icosahedron-type structure. Icosahedral R -Mg-Zn phases melt incongruently, i.e., they decompose before melting. Investigations of the thermal and transport properties of these phases have previously been carried out on polygrain and often multiphase samples. Recent advances in the growth of single-grain R -Mg-Zn quasicrystals,⁴ which were based on the ternary phase diagram reported by Langsdorf and co-workers,⁵ have eliminated the occurrence of second phases and effects of grain boundaries upon the measured properties. The structural quality of these single-grain quasicrystals, as revealed by recent high-resolution transmission electron microscopy

(HRTEM) and x-ray-diffraction experiments sets them among the best highly ordered icosahedral phases.⁶

In view of the high structural perfection and the rather low electrical resistivities that fall in the range between 150 and 200 $\mu\Omega \text{ cm}$,⁷ i.e., distinctly lower than the values previously reported for other thermodynamically stable icosahedral phases, single-grain R -Mg-Zn quasicrystals may be classified as highly ordered icosahedral metals, thus not corroborating the views that structurally perfect icosahedral phases are either poor conductors or insulators. In order to gain a better understanding of the ground state of the icosahedral R -Mg-Zn phases, it seemed of interest to investigate the low-temperature electronic and thermal properties. Here we report the results of measurements of thermal (specific heat), electrical transport (electrical conductivity, magnetoconductivity, Hall effect) and optical properties (reflectivity) of single-grain quasicrystals of icosahedral Y-Mg-Zn in different temperature ranges between 1.5 and 300 K. We also present results for the specific heat and optical reflectivity of icosahedral Tb-Mg-Zn.

II. SAMPLES AND EXPERIMENTS

Single-grain quasicrystals of icosahedral Y-Mg-Zn and Tb-Mg-Zn with sizes of up to 5 mm were grown by slow cooling of ternary melts containing excess magnesium and zinc.⁴ For Y-Mg-Zn the starting composition was chosen based on the primary solidification area of the icosahedral phase, as identified by Langsdorf and co-workers.⁵ Some ad-

justment of the starting composition was necessary to grow icosahedral Tb-Mg-Zn.⁴ Following the growth, the undecanted flux was removed from the surface by a dilute solution of nitric acid in methanol. Using quantitative x-ray microanalysis, the composition of the Tb-Mg-Zn single grains was found to be 9 at.% Tb, 34 at.% Mg, and 57 at.% Zn,⁴ i.e., very close to the composition of icosahedral Y-Mg-Zn reported in Ref. 5. The specimens were cut from the single quasicrystals using spark-erosion. Thermal and optical measurements were performed on the specimens in the form of plates with approximate dimensions $3 \times 3 \times 1$ mm. A specimen of icosahedral Y-Mg-Zn in the form of a prism $0.4 \times 0.4 \times 3$ mm in size was used for electrical transport measurements. Both Y-Mg-Zn specimens were cut from adjacent parts of the same single-grain quasicrystal.

The electrical conductivity, the magnetoconductivity, and the Hall effect were measured by a standard low-frequency ac technique in different temperature ranges between 1.8 and 250 K and in magnetic fields of up to 70 kOe. The magnetoconductivity was measured in a transverse configuration, i.e., the magnetic field \mathbf{H} was applied perpendicular to the electrical current \mathbf{I} . For the Hall effect measurement, a standard setup with the two Hall voltage contacts fixed along a line perpendicular both to the current \mathbf{I} and to the magnetic field \mathbf{H} was used. A capacitance thermometer was used to stabilize the temperature, and at each temperature point, the magnetic field was varied stepwise. In order to eliminate the misalignment voltage, at each magnetic field setting, the Hall voltage was measured with the sample in two different orientations, 180° apart.

A conventional relaxation-type method was used for the specific-heat $C_p(T)$ measurements. A sapphire disk onto which a heater and a Ge-Au thermometer had been evaporated was weakly thermally coupled to a heat sink held at a constant temperature. The samples were mounted on the disk using a thin layer of Apiezon grease. The temperatures in the range between 1.5 and 20 K were reached in a pumped ⁴He cryostat.

The optical reflectivity $R(\omega)$ has been measured in the frequency range between 16 and 9.7×10^4 cm^{-1} , i.e., over almost four orders of magnitude in frequency, using four spectrometers with overlapping frequency ranges. In the far-infrared range (FIR) we used a Bruker IF113v Fourier interferometer with a Hg arc-light source and a He-cooled Gebolometer detector, while from the FIR up to the midinfrared range a fast-scanning Bruker interferometer IFS48PC was used. A homemade spectrometer based on a Zeiss monochromator and a McPherson spectrometer were employed in the visible spectral range and in the ultraviolet spectral range, respectively. From the midinfrared down to the FIR we have used the reflectivity of gold as reference. All measurements have been made at 300 K and in the FIR range also at selected fixed temperatures between 6 and 300 K. Upon completing the measurements, the surfaces of both samples were polished and the measurements were performed again, without any noticeable change in the $R(\omega)$ data.

III. RESULTS, ANALYSIS, AND DISCUSSION

A. Electrical transport in icosahedral Y-Mg-Zn

1. Electrical conductivity and magnetoconductivity

Our electrical conductivity $\sigma(T)$ data for Y-Mg-Zn taken in nominally zero magnetic field between 1.8 and 150 K is

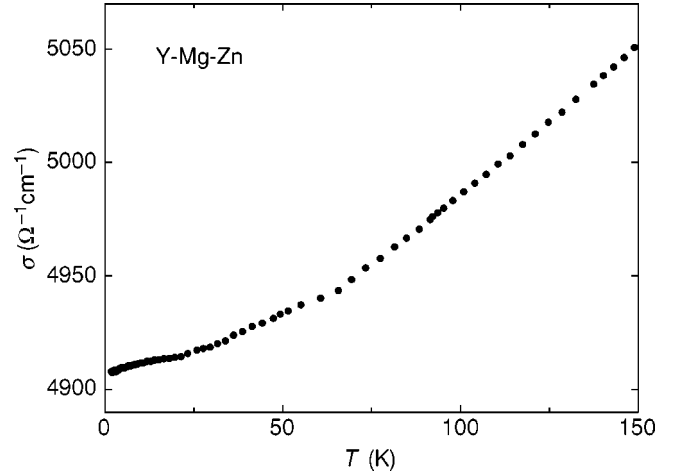


FIG. 1. Electrical conductivity σ of a single-grain quasicrystal of icosahedral Y-Mg-Zn as a function of temperature T between 1.8 and 150 K.

displayed in Fig. 1. Within this temperature range, the overall variation of the conductivity σ amounts to 3% of the total conductivity. In the whole covered temperature range σ increases monotonically with increasing T . A tendency to a decreasing slope $d\sigma/dT$ is evident above approximately 5 K and at 14 K the $\sigma(T)$ curve exhibits an inflection point. Above 14 K, the slope $d\sigma/dT$ of the conductivity curve increases with increasing temperature T . The shape of the $\sigma(T)$ curve and the conductivity values are close to those previously reported for single-grain quasicrystals of icosahedral Y-Mg-Zn.⁷ As we shall discuss below, the observed behavior of $\sigma(T)$ above 14 K can *quantitatively* be described by considering weak-localization effects in the presence of spin-orbit scattering. A contribution to $\sigma(T)$ due to another mechanism is necessary, however, to account for the temperature variation of the conductivity $\sigma(T)$ between 1.8 and 14 K.

The magnetoconductivity $\delta\sigma(H)$ data taken at selected fixed temperatures in the range between 4 and 30 K and in magnetic fields of up to 70 kOe are shown in Fig. 2. Because $\delta\sigma(H)$ is obtained as the small difference between two large quantities $\sigma(H)$ and $\sigma(0)$, which are inversely proportional to extremely small measured voltages along the sample, the scatter of the data points is considerable. At 4 K and at 7.8 K, $\delta\sigma(H)$ first is increasingly negative with increasing magnetic field H , passes through a minimum, and then tends to positive values with further increasing H , changing sign near 4.3 and 3.3 kOe, respectively. For $T=20$ and 30 K, $\delta\sigma$ is positive in the whole covered magnetic-field range and increases monotonously with increasing magnetic field H . This $\delta\sigma(H)$ behavior may be interpreted as a manifestation of quantum-interference effects when spin-orbit scattering is present. We recall that in the weak-localization regime, quantum-interference effects give a magnetoconductivity $\delta\sigma(H)$ that is positive when the spin-orbit scattering is weak, i.e., $\tau_{\text{so}}^{-1} \ll \tau_{\text{i}}^{-1}$, where τ_{so}^{-1} and τ_{i}^{-1} denote the spin-orbit and inelastic scattering rate, respectively. In the intermediate regime $\tau_{\text{so}}^{-1} \sim \tau_{\text{i}}^{-1}$ the magnetoconductivity $\delta\sigma(H)$ changes sign from negative to positive with increasing magnetic field and it remains negative in the limit of strong spin-orbit scattering $\tau_{\text{so}}^{-1} \gg \tau_{\text{i}}^{-1}$.⁸ For Y-Mg-Zn, the magnetocon-

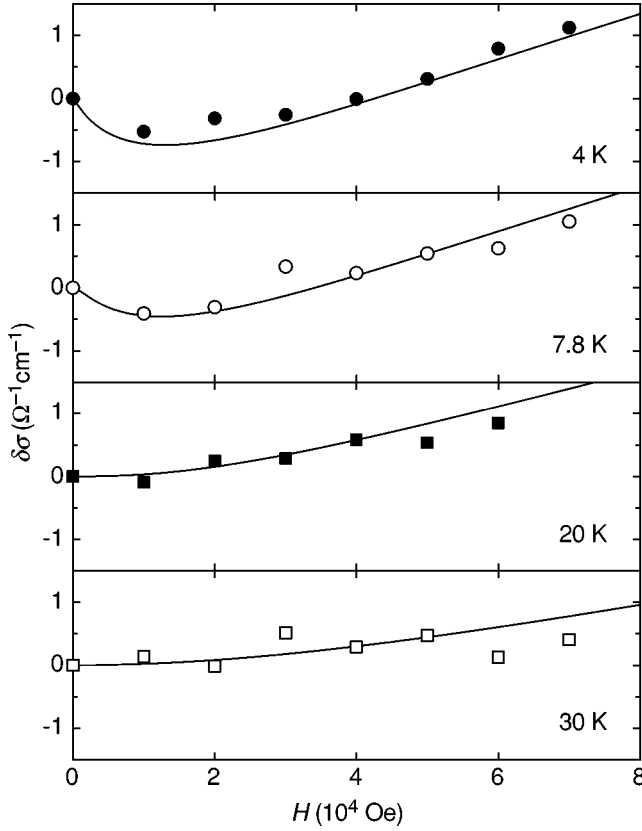


FIG. 2. Magnetoconductivity $\delta\sigma$ of Y-Mg-Zn as a function of magnetic field H at selected fixed temperatures in the range between 4 and 30 K. The solid lines are fits of Eq. (4) to the $\delta\sigma(H)$ data, as explained in the text.

ductivity $\delta\sigma(H)$ curves taken below 8 K are characteristic for moderate spin-orbit scattering $\tau_{so}^{-1} \sim \tau_i^{-1}$. Above 20 K, however, the $\delta\sigma(H)$ data indicate that spin-orbit scattering is now weak, i.e., $\tau_{so}^{-1} \ll \tau_i^{-1}$. A crossover from the regime of moderate spin-orbit scattering to the regime of weak spin-orbit scattering, reflected by a change in the type of the $\delta\sigma$ vs H variation, occurs because the inelastic scattering rate τ_i^{-1} rapidly increases with increasing temperature T .

We first analyze the temperature variation of the conductivity $\sigma(T)$ measured in zero magnetic field between 1.8 and 150 K, and subsequently discuss the behavior of the low-temperature magnetoconductivity $\delta\sigma(H)$. The weak-localization correction in the presence of spin-orbit scattering is given by⁹

$$\delta\sigma_{WL}(T) = \frac{e^2}{2\pi^2\hbar} \left(3 \sqrt{\frac{1}{D\tau_{so}} + \frac{1}{4D\tau_i}} - \sqrt{\frac{1}{4D\tau_i}} - 3 \sqrt{\frac{1}{D\tau_{so}}} \right), \quad (1)$$

where D is the electron diffusion constant. In Eq. (1), the last temperature-independent term is commonly added so that $\delta\sigma_{WL}(T)$ tends to 0 at $T=0$. The electron diffusion constant D may be estimated using the Einstein relation for the electrical conductivity $\sigma_B = e^2 N(E_F) D$, where σ_B is the classical Boltzmann conductivity and $N(E_F)$ is the density of electronic states at the Fermi energy. With $N(E_F) = 0.263$ states

$eV^{-1} \text{atom}^{-1}$, calculated from the Sommerfeld coefficient $\gamma_{el} = 0.623 \text{ mJ mol}^{-1} \text{K}^{-2}$, as obtained from the low-temperature specific-heat measurements performed on a sample cut from the same single grain of icosahedral Y-Mg-Zn (see Sec. III B) and assuming that $\sigma_B = \sigma(0)$, where $\sigma(0) = 4.91 \times 10^3 \text{ } \Omega^{-1} \text{cm}^{-1}$ is the residual conductivity, we estimate the electron diffusion constant D to be $2.24 \text{ cm}^2/\text{s}$. We note that the weak-localization effects may, in principle, lead to a difference between the Boltzmann conductivity σ_B at zero temperature and the residual conductivity $\sigma(0)$. Considering the residual conductivity ratio that is very close to unity and the rather large value of the electron diffusion constant D , the relative uncertainty in our estimate of D is expected to be small, however.

We first focus on the influence of spin-orbit scattering on the conductivity in the regime of weak localization. Spin-orbit scattering leads to weak antilocalization, which is manifest as a region of negative slope $d\sigma/dT$ of the $\sigma(T)$ curve at the lowest temperatures where $\tau_i^{-1}(T) \ll \tau_{so}^{-1}$. A crossover between the regime of weak antilocalization to the regime of weak localization leads to a shallow minimum in the $\sigma(T)$ curve. The depth of this minimum at T_{\min} where $\tau_{so}^{-1} = 2\tau_i^{-1}$, is

$$\delta\sigma_{WL}(0) - \delta\sigma_{WL}(T_{\min}) = (3 - 2\sqrt{2}) \frac{e^2}{2\pi^2\hbar} \frac{1}{\sqrt{D\tau_{so}}}. \quad (2)$$

Above T_{\min} , the weak-localization correction $\delta\sigma_{WL}(T)$ to the conductivity increases with increasing T . At high temperatures where $\tau_i^{-1}(T) \gg \tau_{so}^{-1}$, $\delta\sigma_{WL}(T)$ no longer depends on τ_{so}^{-1} and Eq. (1) reduces to

$$\delta\sigma_{WL}(T) = \frac{e^2}{2\pi^2\hbar} \frac{1}{\sqrt{D\tau_i}}. \quad (3)$$

The temperature variation of the electrical conductivity σ in the weak-localization regime is determined by the inelastic scattering rate $\tau_i^{-1}(T)$,¹⁰ which is assumed to follow a simple power law $\tau_i^{-1} \propto T^p$. The value of the exponent p is determined by the dominant scattering mechanism. Electron-phonon scattering is expected to lead to $p=3$ and $p=2$ for pure and dirty metals, respectively.^{8,11,12} An exponent $p=2$ is predicted for electron-electron scattering in pure metals,⁸ whereas electron-electron scattering in impure metals has been claimed to yield $p=3/2$.^{13,14} For Y-Mg-Zn, a stronger than linear-in-temperature variation of the electrical conductivity $\sigma(T)$ indicates that $p > 2$. As we discussed above, our $\delta\sigma(H)$ curves indicate that a crossover from the regime of moderate spin-orbit scattering $\tau_i^{-1} \sim \tau_{so}^{-1}$ to the regime of weak spin-orbit scattering $\tau_i^{-1} \gg \tau_{so}^{-1}$ occurs at a temperature between 7.8 and 20 K. In the regime of weak spin-orbit scattering, the weak-localization correction $\delta\sigma_{WL}(T)$ is expected to vary as $\tau_i^{-1/2}$ [see Eq. (3)]. Assuming that the inelastic scattering rate can indeed be described by a simple power law $\tau_i^{-1} \propto T^p$ we obtain $\delta\sigma_{WL} \propto T^{p/2}$. Our σ data plotted versus $T^{3/2}$ between 20 and 150 K in Fig. 3 reveals the data points to lie along a straight line, thus indicating that the inelastic scattering rate τ_i^{-1} varies as T^3 . Fitting Eq. (3) to our $\sigma(T)$ data between 20 and 150 K and assuming $\tau_i^{-1} = bT^3$ yields $b = (9.4 \pm 0.3) \times 10^7 \text{ s}^{-1} \text{K}^{-3}$. The result of the

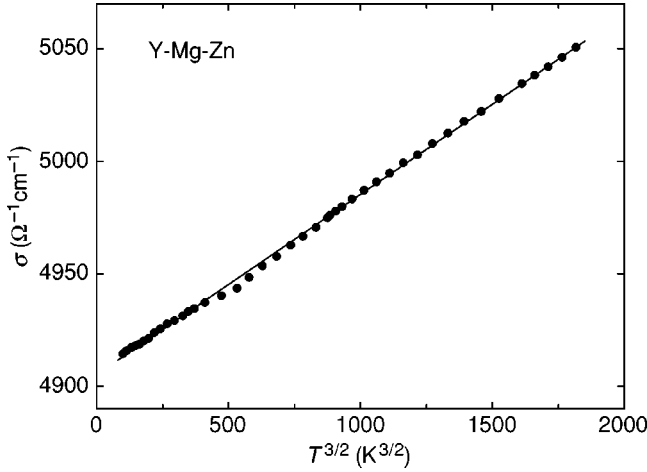


FIG. 3. Electrical conductivity σ of icosahedral Y-Mg-Zn plotted vs $T^{3/2}$. The straight line is the fit of Eq. (3) to the $\sigma(T)$ data between 20 and 150 K (see text).

fit is shown as the straight line in Fig. 3. We note that the cubic-in-temperature variation of τ_i^{-1} is consistent with electron-phonon scattering in pure metals, a scenario that is quite remarkable considering the quasiperiodic nature of Y-Mg-Zn. As we shall discuss below, also our $\delta\sigma(H)$ data are consistent with $\tau_i^{-1} \propto T^3$.

We now discuss the electrical conductivity data below 20 K. The monotonous $\sigma(T)$ variation with the positive slope $d\sigma/dT$ implies that $2\tau_i^{-1}(T) > \tau_{so}^{-1}$ above 1.8 K. Our $\delta\sigma(H)$ data indicate, however, that $\tau_i^{-1}(T)$ is of similar magnitude as τ_{so}^{-1} at a temperature in the range between 7.8 and 20 K. As we shall discuss below, based on the analysis of our magnetoconductivity data $2\tau_i^{-1}$ is equal to τ_{so}^{-1} at 13 K. Accordingly, the slope $d\sigma/dT$ of the $\sigma(T)$ curve is expected to turn negative below that temperature, quite in contrast with our observations. Thus, our low-temperature $\sigma(T)$ data cannot be described by a contribution from weak-localization effects alone. The monotonous $\sigma(T)$ variation and the weakening of the slope $d\sigma/dT$ around an inflection point at 14 K may be related to a crossover, with decreasing temperature, to a regime in which $\sigma(T)$ is affected by Coulomb interactions among itinerant electrons.¹⁴ Indeed, in the temperature range below several degrees Kelvin, the interaction correction varying as \sqrt{T} often dominates $\sigma(T)$ of quasicrystals with fci structures. Examples are icosahedral Al-Cu-Fe,¹⁵ Al-Mn-Pd,¹⁶ and also Al-Re-Pd provided its residual conductivity $\sigma(0)$ is not too low.¹⁷ More recently, a square-root temperature dependence of the electrical conductivity has been reported for a multigrain sample of icosahedral Y-Mg-Zn obtained via conventional solidification.¹⁸ Considering our $\sigma(T)$ data between 1.8 and 20 K, the contributions to the electrical conductivity $\sigma(T)$ from the weak-localization term and from the Coulomb interaction term cannot be separated in simple ways. This is mainly because the Coulomb interaction term is expected to weaken with increasing temperature, finally vanishing in the temperature range between 10 and 50 K.¹⁹

We now compare our low-temperature magnetoconductivity $\delta\sigma(H)$ data with theoretical calculations considering a contribution to the magnetoconductivity due to quantum interference effects. For systems with large electron diffusion

constants $D > 2 \text{ cm}^2/\text{s}$, the magnetoconductivity in the weak-localization regime and in the presence of spin-orbit scattering is given by⁸

$$\delta\sigma_{\text{WL}}(H) = -\frac{e^2}{2\pi^2\hbar} \sqrt{\frac{eH}{\hbar}} \left[\frac{1}{2} f_3\left(\frac{H}{H_\phi}\right) - \frac{3}{2} f_3\left(\frac{H}{H_2}\right) \right], \quad (4)$$

where

$$f_3(x) = \sum_{n=0}^{\infty} \left[2 \left(n + 1 + \frac{1}{x} \right)^{1/2} - 2 \left(n + \frac{1}{x} \right)^{1/2} - \left(n + \frac{1}{2} + \frac{1}{x} \right)^{-1/2} \right], \quad (5)$$

$$H_\phi = \frac{\hbar}{4eD\tau_i}, \quad (6)$$

and

$$H_2 = \frac{\hbar}{4eD\tau_i} + \frac{4}{3} \frac{\hbar}{4eD\tau_{so}}. \quad (7)$$

The series in Eq. (5) converges very slowly and using this expression directly for analyzing magnetoconductivity data is not practical. Instead, we used the following expression:²⁰

$$f_3(x) \approx 2 \left(\sqrt{2 + \frac{1}{x}} - \sqrt{\frac{1}{x}} \right) - \left[\left(\frac{1}{2} + \frac{1}{x} \right)^{-1/2} + \left(\frac{3}{2} + \frac{1}{x} \right)^{-1/2} \right] + \frac{1}{48} \left(2.03 + \frac{1}{x} \right)^{-3/2}, \quad (8)$$

which was claimed to approximate the function $f_3(x)$ with an accuracy of better than 0.1% for all x and to yield the correct asymptotic limit $f_3(x \rightarrow \infty) = 0.6049$. We fit Eq. (4) to our magnetoconductivity $\delta\sigma(H)$ data taken at 4, 7.8, 20, and 30 K using the electron diffusion constant D and the inelastic scattering time $\tau_i(T)$ evaluated as described above. Although the scattering of the data points is substantial, the $\delta\sigma(H)$ variation is well reproduced by the fits both qualitatively and quantitatively, as may be seen in Fig. 2. This implies that the Coulomb interaction contribution to $\delta\sigma(H)$ is unimportant, at least, in the temperature range and in the magnetic-field range investigated here. The spin-orbit scattering time τ_{so} —the only parameter of these fits—appears to be rather insensitive to the details of the fitting procedure and, therefore, can reliably be determined. The best fits shown in the panels of Fig. 2 as the solid lines are achieved with $\tau_{so} = 2.2 \times 10^{-12} \text{ s}$. We estimate the uncertainty in τ_{so} to be of the order of 20%. The resulting value of τ_{so} is distinctly larger than the values in the range between 1.1×10^{-13} and $1.5 \times 10^{-13} \text{ s}$, previously reported for icosahedral Al-Mn-Pd, a quasicrystal with relatively strong spin-orbit scattering.¹⁶ Our τ_{so} value is of the same order of magnitude as $\tau_{so} = 4 \times 10^{-12} \text{ s}$ reported for icosahedral Al-Cu-Fe, in which the strength of spin-orbit scattering is moderate.¹⁵ This is not at all surprising, because for icosahedral Y-Mg-Zn the weighted average of the atomic weights of constituent elements is close to that of icosahedral Al-Cu-Fe. Finally, we note that our $\delta\sigma(H)$ results are in obvious conflict with a recent claim by Kondo and co-workers¹⁸

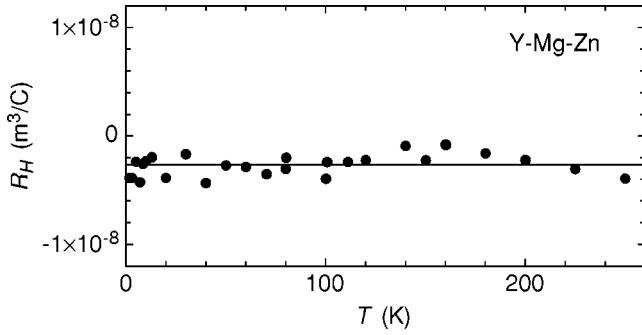


FIG. 4. Hall coefficient R_H of Y-Mg-Zn between 1.8 and 250 K. The horizontal solid line represents the average value of R_H over the whole covered temperature range.

that icosahedral Y-Mg-Zn can be regarded as an electronic system with weak spin-orbit scattering, based on an observation of the positive magnetoconductivity $\delta\sigma$ of melt-spun Y-Mg-Zn in the temperature range between 2.8 and 10 K.

Concluding our discussion, we reiterate that for a single quasicrystal of icosahedral Y-Mg-Zn, the zero field conductivity $\sigma(T)$ between 20 and 150 K and the magnetoconductivity $\delta\sigma(H)$ in magnetic fields of up to 70 kOe taken at selected fixed temperatures in the range between 4 and 30 K, are well described considering quantum-interference effects alone. The obvious absence of a region in which the slope $d\sigma/dT$ of the conductivity $\sigma(T)$ curve is negative is most likely related to a crossover into a low-temperature regime in which $\sigma(T)$ is affected by a sizable Coulomb-interaction correction. The regime, in which the interaction correction dominates the temperature dependence of σ is, however, expected to occur well below the lowest reached temperature of 1.8 K. In this connection, an investigation of the electrical transport properties of Y-Mg-Zn in the millikelvin temperature range might confirm our conjecture.

2. Hall effect

The Hall coefficient R_H was determined from a linear fit to the magnetic-field variation of the Hall resistivity $\rho_H(H)$ at $H \geq 40$ kOe. In Fig. 4, $R_H(T)$ is shown between 1.8 and 250 K. The Hall coefficient R_H takes the values between -1×10^{-9} and -5×10^{-9} m^3/C in the entire covered temperature range. In view of the scattering of the data points, no analysis of the quantum corrections to $R_H(T)$ is attempted. Averaging the $R_H(T)$ data between 1.8 and 250 K yields $(-2.7 \pm 0.2) \times 10^{-9}$ m^3/C , which corresponds to a very low effective charge-carrier concentration $n_{\text{eff}} = (e|R_H|)^{-1} \approx 2.3 \times 10^{21}$ cm^{-3} , or approximately 0.04 charge carriers per atom of the Y-Mg-Zn alloy. A comparative analysis of the specific heat and optical reflectivity data obtained from a sample cut from the same grain of the icosahedral Y-Mg-Zn material also leads to a low itinerant charge-carrier density n_i of about 0.13 charge carriers per atom (see Sec. III C). On the other hand, we note that n_{eff} is distinctly lower than n_i . Given the complexity of the electronic excitation spectrum of icosahedral quasicrystals, the significance of this difference is not quite clear at present. Within a simple two-band model consistent with the Hume-Rothery-type stabilization, the small ratio $n_{\text{eff}}/n_i \approx 0.3$ may indicate that icosahedral Y-Mg-Zn is a nearly compensated

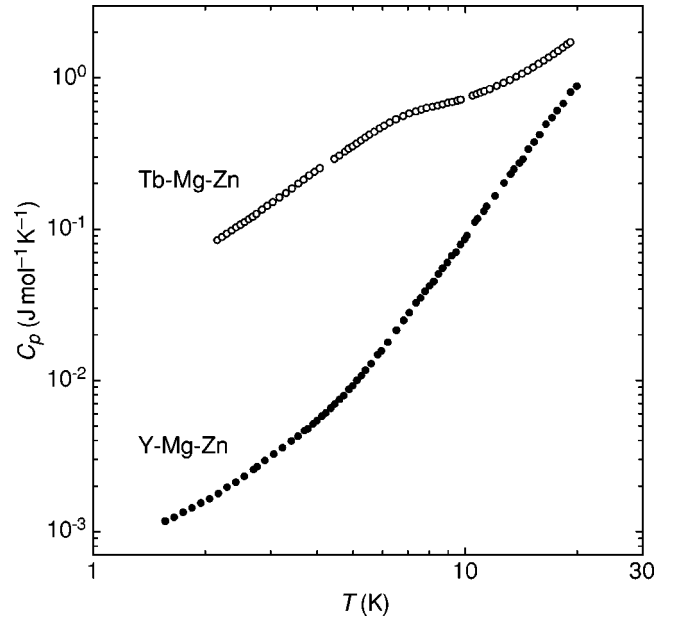


FIG. 5. Specific heat $C_p(T)$ of icosahedral Y-Mg-Zn and Tb-Mg-Zn between 1.5 and 20 K plotted on logarithmic scales.

metal. In this connection, we recall that the regime of near compensation has previously been claimed by Lindqvist and co-workers²¹ for icosahedral Al-Cu-Fe, based on the results of Hall effect measurements. Finally, we note that the sign of R_H indicates that the itinerant carriers are predominantly negatively charged, i.e., electronlike.

B. Specific heat

1. Y-Mg-Zn

The specific-heat $C_p(T)$ data for icosahedral Y-Mg-Zn measured in the temperature range between 1.5 and 20 K is shown in Fig. 5 on a double logarithmic plot. Between 1.5 and 4 K our $C_p(T)$ data, shown in Fig. 6 as C_p/T vs T^2 , are very well fitted by a sum of a linear- and a cubic-in-temperature term

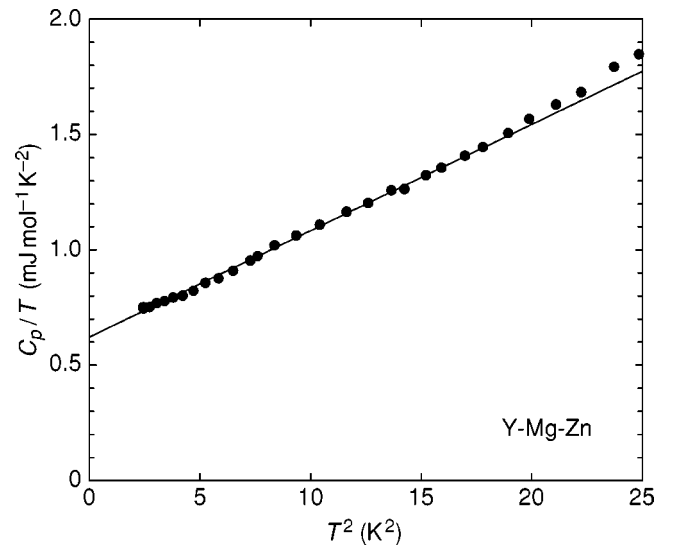


FIG. 6. C_p/T vs T^2 for icosahedral Y-Mg-Zn. The solid line indicates the fit of Eq. (9) to the $C_p(T)$ data (see text).

$$C_p(T) = \gamma T + \beta T^3. \quad (9)$$

The fit is shown as the solid line through the data points of Y-Mg-Zn in Fig. 6. The fitting parameters are $\gamma = (0.623 \pm 0.004) \text{ mJ mol}^{-1} \text{ K}^{-2}$ and $\beta = (46.1 \pm 0.5) \mu\text{J mol}^{-1} \text{ K}^{-4}$. Our value of the parameter γ is close to analogous value reported previously for a polycrystalline sample of Y-Mg-Zn, prepared via conventional solidification.²²

A linear-in-temperature term γT in the low-temperature specific heat of metals is commonly associated with excitations of electronic degrees of freedom. For icosahedral quasicrystals, however, a reliable evaluation of the electronic contribution $\gamma_{\text{el}} T$ to the specific heat $C_p(T)$ is hampered by the presence of tunneling states, as indicated by the results of experiments probing sound velocities, acoustic attenuation, and thermal conductivity at low temperatures.²³⁻²⁵ In the formalism of the tunneling-states model^{26,27} the spectral density of tunneling states is assumed to be energy independent and limited to a certain energy range. In this case thermal excitations of tunneling states are also expected to contribute a linear-in-temperature term $C_{\text{TS}} = \gamma_{\text{TS}} T$ to the total specific heat $C_p(T)$.^{26,27} Accordingly, in an analysis of the specific heat $C_p(T)$ data of an icosahedral phase, contributions from both electronic and tunneling-state excitations must be considered. Tunneling states are commonly present in metallic glasses and their contribution $C_{\text{TS}}(T)$ to the total specific heat $C_p(T)$ is typically of the order $0.05 T \text{ mJ mol}^{-1} \text{ K}^{-1}$.²⁸ This $\gamma_{\text{TS}} T$ value corresponds to approximately 8% of the linear contribution γT to the specific heat $C_p(T)$ of icosahedral Y-Mg-Zn. Recent low-temperature investigations of the thermal conductivity and of the sound velocities performed on single quasicrystals of icosahedral Y-Mg-Zn did not reveal, however, any distinct features in the temperature variation of these quantities that were characteristic of interactions of acoustic excitations with tunneling states.^{29,30} Therefore, it is reasonable to assume that the linear term γT in the low-temperature specific heat $C_p(T)$ of icosahedral Y-Mg-Zn is almost entirely due to the electronic excitations, i.e., $\gamma T = \gamma_{\text{el}} T$.

For icosahedral Y-Mg-Zn, the value of the electronic specific-heat parameter γ_{el} is somewhat higher than the γ_{el} values previously reported for fcc quasicrystals in the Al-Mn-Pd and Al-Re-Pd systems, which fall into the range between 0.11 and 0.41 $\text{mJ mol}^{-1} \text{ K}^{-2}$.^{17,24,31} For these materials, the small electronic specific heat has tentatively been attributed to the presence of a pseudogap in the density of electronic states (DOS) at the Fermi energy E_F .^{17,24,31} The pseudogap in the electronic DOS at E_F of the icosahedral Al-Mn-Pd and Al-Re-Pd quasicrystals was also inferred from the analysis of the optical conductivity spectra obtained from the same samples.^{17,32} Based on our low-temperature specific-heat results, we cannot claim a low DOS at the Fermi energy E_F because the value of the electronic specific-heat parameter γ_{el} of icosahedral Y-Mg-Zn is close to that of zinc. The optical conductivity spectrum of Y-Mg-Zn to be discussed in detail in Sec. III C exhibits a distinct feature that is characteristic of excitations across a pseudogap, however.

We now focus on the low-temperature specific-heat $C_{\text{ph}}(T)$ due to lattice excitations. At low temperatures only excitations of the long-wavelength acoustic modes contribute to $C_{\text{ph}}(T)$, which is given by

$$C_{\text{ph}}(T) = \frac{2\pi^2 k_B^4}{5\hbar^3} \frac{T^3}{v_s^3}, \quad (10)$$

where $1/v_s^3$ is the average, over the directions of propagation, of the inverse third power of the phase velocities $v_i(\mathbf{q})$ of the three acoustic modes. The coefficient $\beta = 46.1 \mu\text{J mol}^{-1} \text{ K}^{-4}$, matching the cubic-in-temperature term of the low-temperature specific heat of icosahedral Y-Mg-Zn leads to a thermodynamic average of the sound velocities $v_s^{\text{th}} = 3.04 \times 10^5 \text{ cm/s}$. The low-temperature lattice specific heat of periodic crystals is often characterized by the Debye temperature Θ_D . We note, however, that a common definition of Θ_D involves the number of atoms per unit cell and thus cannot be applied to a quasicrystalline crystal. Defining the Debye temperature Θ_D of a quasicrystal as

$$\Theta_D = \frac{\hbar}{k_B} (6\pi^2 n_a)^{1/3} v_s, \quad (11)$$

where n_a is the number of atoms per unit volume, we deduce the thermodynamic Θ_D^{th} Debye temperature of icosahedral Y-Mg-Zn to be 348 K.

2. Tb-Mg-Zn

Also our specific heat $C_p(T)$ data for Tb-Mg-Zn in the temperature range between 2 and 19 K is displayed in Fig. 5, indicating a large excess specific heat $C_{\text{ex}}(T)$ if compared to $C_p(T)$ of Y-Mg-Zn. It is obvious that $C_{\text{ex}}(T)$ is the dominant contribution to $C_p(T)$ of the Tb-based quasicrystal within the whole covered temperature range, thus complicating a direct analysis of the specific-heat data of this material. The excess specific heat C_{ex} may be obtained by subtracting the electronic term C_{el} and the lattice term C_{ph} , evaluated from the specific-heat data of the Y-Mg-Zn phase, from the total measured specific heat C_p . The structure, as determined by the x-ray diffraction and HRTEM investigations, is the same for both icosahedral phases. Assuming only a small contribution of the f electrons to the density of electronic states at the Fermi energy E_F , one may expect that the electronic term C_{el} is only slightly affected by the substitution of Y by Tb. Considering in addition that the six-dimensional lattice parameters and, consequently, real-space interatomic distances differ very little, one may further expect that the lattice stiffness is nearly the same for both phases. In this case, the main difference between the lattice contributions C_{ph} to the specific heat is due to differences in atomic masses, i.e., $C_{\text{ph}} \propto M^{3/2}$, where M is the mean atomic mass. With $M_{\text{Tb-Mg-Zn}}/M_{\text{Y-Mg-Zn}} = 1.113$ we obtain $C_{\text{ph, Tb-Mg-Zn}} = 1.175 C_{\text{ph, Y-Mg-Zn}}$. Over the entire covered temperature range, C_p of the Tb alloy exceeds the sum of C_{el} and C_{ph} by at least a factor of 2, and therefore our evaluation of C_{ex} is expected to be quite reliable. The resulting excess specific heat $C_{\text{ex}}(T)$ is shown in Fig. 7.

Based on the results of our dc magnetic susceptibility measurements reported in Ref. 7, single-grain quasicrystals of icosahedral Tb-Mg-Zn exhibit a spin-glass-type freezing of Tb moments at $T_f = 5.8 \text{ K}$. Therefore, at least part of the excess specific heat $C_{\text{ex}}(T)$ must be attributed to spin-glass-type magnetic excitations. For spin-glass systems, the magnetic specific heat $C_m(T)$ at $T=0$ starts off with a tempera-

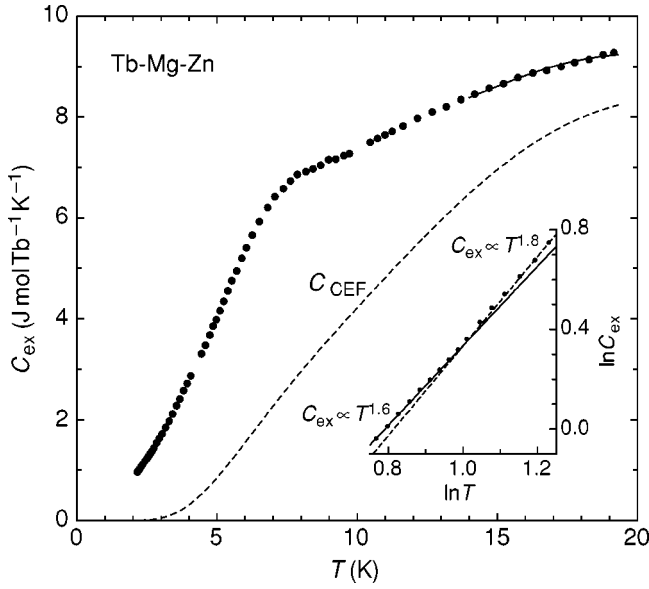


FIG. 7. The excess specific heat $C_{\text{ex}}(T)$ of icosahedral Tb-Mg-Zn. The solid line is the fit of Eq. (12) to the data between 14 and 19 K. The broken line indicates the CEF contribution $C_{\text{CEF}}(T)$ to the specific heat. Inset: $\ln C_{\text{ex}}$ vs $\ln T$ between 2 and 3.5 K; the solid line and the broken line are the linear fits to the data between 2 and 2.4 K, and between 3 and 3.5 K, respectively.

ture variation of the form $C_m \propto T^a$, where the exponent a usually takes values between 1.2 and 1.7,^{33,34} reaches a maximum at a temperature T_{max} that is somewhat higher than the freezing temperature T_f and decreases with further increasing T , approaching a T^{-2} variation well above T_{max} .³⁵ We note, however, that after passing through a shoulder-type feature at 7 K, C_{ex} continues to rise with increasing temperature, indicating that in addition to C_m , the excess specific heat C_{ex} contains another contribution, which gains in weight towards higher temperatures. We attribute this contribution to excitations to higher levels of the crystal-electric-field (CEF) split multiplet of the $4f$ -electron Hund's rule ground state. We have previously reported that CEF effects lead to a significant local magnetic anisotropy of Tb^{3+} ions, which manifests itself by higher freezing temperatures T_f of the $(\text{Y}_{1-x}\text{Tb}_x)\text{-Mg-Zn}$ solid solutions than for the $(\text{Y}_{1-x}\text{Gd}_x)\text{-Mg-Zn}$ alloys with the same heavy rare-earth concentrations x .⁷

A rigorous analysis of the CEF contribution $C_{\text{CEF}}(T)$ to the specific heat $C_p(T)$ of Tb-Mg-Zn meets difficulties. This is mainly because the fci quasilattices allow multiple inequivalent sites for the same atomic species and, although simulations of the HRTEM images have indicated that the rare-earth atoms preferentially occupy the center of an icosahedron decorated by Mg and Zn,⁶ the point symmetries of the rare-earth sites are not really known at present. Most likely, icosahedral shells are not decorated completely by either Mg or Zn, thus leading to rather low point symmetries of the rare-earth sites and, consequently, to a singlet or, at most doubly degenerate ground state of Tb^{3+} ions.

At the lowest temperatures between 2 and 3.5 K, the slope $d \ln C_{\text{ex}} / d \ln T$ of the $\ln C_{\text{ex}}$ vs $\ln T$ curve shown in the inset of Fig. 7 increases from 1.6 to 1.8. We attribute this stronger than power-law variation of $C_{\text{ex}}(T)$ to an onset of the CEF

term $C_{\text{CEF}}(T)$. The magnitude of the $C_{\text{ex}}(T)$ deviation from the approximate $T^{1.6}$ variation of the low-temperature spin-glass magnetic contribution C_m is compatible with a minimum splitting Δ/k_B in the range between 25 and 35 K between the lowest and first excited levels of the CEF-split $J = 6$ multiplet of Tb^{3+} ions. On the other hand, the monotonous $C_{\text{ex}}(T)$ variation with a positive slope dC_{ex}/dT up to the highest measured temperature of 19 K reveals excitations to levels separated from the lowest level by more than 50 K.

For our more detailed analysis of the $C_{\text{ex}}(T)$ data we have assumed that the main contributions to the excess specific heat $C_{\text{ex}}(T)$ are from spin-glass-type magnetic excitations and from excitations to higher levels of the CEF-split ground-state multiplet of Tb^{3+} ions. Assuming further that in the temperature range covered in our experiment, $C_{\text{CEF}}(T)$ may be approximated by a Schottky-type anomaly resulting from excitations out of a ground-state doublet to levels of unknown degeneracy around two higher energies, the excess specific heat well above T_{max} may be written as

$$C_{\text{ex}}(T) = \frac{A}{T^2} + R \left(\frac{\Delta}{Zk_B T} \right)^2 \left\{ Z \left[\sum_{i=1}^3 g_i \Delta_i^2 \exp\left(-\frac{\Delta_i}{k_B T}\right) \right] - \left[\sum_{i=1}^3 g_i \Delta_i \exp\left(-\frac{\Delta_i}{k_B T}\right) \right]^2 \right\}, \quad (12)$$

where g_i and Δ_i are the degeneracy and the energy of the i th level, respectively, and

$$Z = \sum_{i=1}^3 g_i \exp\left(-\frac{\Delta_i}{k_B T}\right) \quad (13)$$

is the partition function. The best fit of Eq. (12) to our $C_{\text{ex}}(T)$ data in the temperature range between 14 and 19 K is obtained with $g_1 = 2$, as assumed, $g_2 = 2$ and $g_3 = 7$, yielding $A = (3.7 \pm 0.4) \times 10^2$ J K/mol Tb, $\Delta_2/k_B = (29 \pm 1)$ K and $\Delta_3/k_B = (76 \pm 2)$ K. The result of this fit is displayed as the solid line in Fig. 7. The broken line indicates the CEF contribution $C_{\text{CEF}}(T)$ separately.

The magnetic specific heat C_m of icosahedral Tb-Mg-Zn may now be obtained by subtracting the CEF term C_{CEF} from the excess specific heat C_{ex} . Its temperature dependence is shown in Fig. 8. Between 2 and 3.5 K, C_m varies as T^a with $a = 1.57 \pm 0.01$. This variation, consistent with spin-glass behavior, is illustrated in the inset of Fig. 8, where we plot C_m as a function of T on logarithmic scales. The magnetic specific heat $C_m(T)$ exhibits a maximum at $T_{\text{max}} = 7.2$ K. This temperature is about 25% higher than the freezing temperature $T_f = 5.8$ K, determined from the dc magnetic susceptibility data,⁷ again a typical feature of spin glasses. Our $C_m(T)$ data, in the form of C_m/T vs T , is plotted in Fig. 9. The temperature derivative of the magnetic entropy $dS_m/dT = C_m/T$ reaches a maximum very close to the freezing temperature T_f , indicating that the freezing of the magnetic moments at T_f manifests itself with a maximum change in the magnetic entropy. Although this behavior of the magnetic specific heat $C_m(T)$ is not universal for spin glasses, we note that a coincidence of the maximum in the C_m/T vs T curve and T_f has previously been reported for

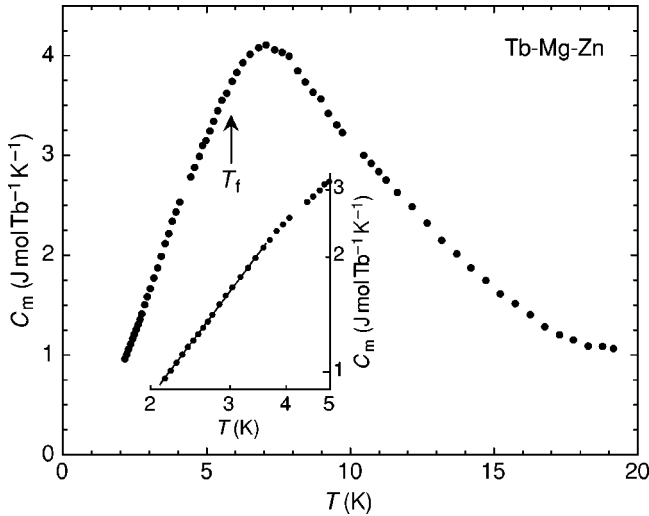


FIG. 8. The calculated magnetic contribution $C_m(T)$ to the specific heat of the Tb-Mg-Zn alloy. Inset: C_m vs T between 2 and 5 K plotted on logarithmic scales; the solid line is the power-law approximation of the data between 2 and 3.5 K, as explained in the text.

icosahedral Al-Mn-Pd.³¹ The magnetic entropy $\Delta S_m(T)$, obtained from the magnetic contribution $C_m(T)$ to the specific heat via

$$\Delta S_m(T) = \int_0^T \frac{C_m}{T'} dT', \quad (14)$$

is displayed in Fig. 10. For this calculation, C_m was extrapolated to zero temperature assuming the power-law variation $C_m(T) \propto T^{1.57}$ below 2 K. The $\Delta S_m(T)$ curve reveals that more than 55% of ΔS_m is released above the freezing temperature T_f . Thus, the freezing of magnetic moments at T_f removes only a fraction of the magnetic entropy, implying a considerable short-range order of magnetic moments above T_f , again typical of spin glasses. At 19 K, ΔS_m reaches $6.1 \text{ J mol Tb}^{-1} \text{ K}^{-1}$. This value is close to $R \ln 2$, thus indicating that the spin-glass-type freezing of Tb moments at $T_f = 5.8 \text{ K}$ indeed involves a doubly degenerate ground state.

C. Optical properties

The optical properties of quasicrystals were frequently studied in recent years and have proven to be very useful for the determination of the charge excitation spectrum.^{17,32,36–38} Generally speaking, the electrodynamic response of a quasicrystal is quite different from that of either a metal or a semiconductor. A common feature in the excitation spectra of both icosahedral and decagonal quasicrystals is an absorption feature at about 10^4 cm^{-1} , overlapping with an effective metallic contribution at low frequencies. The metallic contribution is more pronounced in decagonal than in icosahedral quasicrystals, mainly because of generally higher charge-carrier densities in decagonal phases.^{17,32,36–38} The absorption at about 10^4 cm^{-1} is commonly ascribed to excitations across a pseudogap, the lowest-energy electronic interband transition, possibly a consequence of the Hume-Rothery-type electronic stabilization mechanism.^{17,32,36,39}

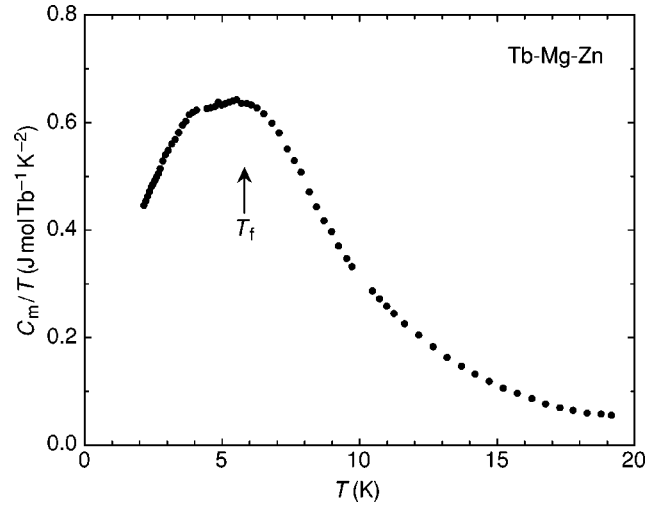


FIG. 9. C_m/T vs T of icosahedral Tb-Mg-Zn.

Figure 11 displays the complete reflectivity $R(\omega)$ spectra for the Y-Mg-Zn and Tb-Mg-Zn quasicrystals at room temperature. The inset highlights the $R(\omega)$ variation in the far infrared (FIR) spectral range. We did not observe any temperature dependence of the $R(\omega)$ spectra, in agreement with the very weak temperature variation of the electrical conductivity $\sigma(T)$.⁷ The complex optical conductivity $\sigma(\omega) = \sigma_1(\omega) + i\sigma_2(\omega)$ was obtained by a standard Kramers-Kronig transformation of the optical reflectivity $R(\omega)$, extrapolated both to lower and to higher frequencies. The extrapolation of $R(\omega)$ to lower frequencies was based on the Hagen-Rubens relation $1 - R(\omega) \propto (\omega/\sigma_{dc})^{1/2}$, i.e., assuming metallic behavior (see inset of Fig. 11). The following scheme for the extrapolation of the optical reflectivity $R(\omega)$ to high frequencies was adopted. Between the highest achieved frequency of $9.7 \times 10^4 \text{ cm}^{-1}$, accessible by our ultraviolet range spectrometer and $3 \times 10^5 \text{ cm}^{-1}$, we assumed $R(\omega) \propto \omega^{-2}$, simulating interband transitions. Above $3 \times 10^5 \text{ cm}^{-1}$, we assumed the behavior of free electrons, i.e., $R(\omega) \propto \omega^{-4}$. The resulting optical conductivity $\sigma_1(\omega)$ spectra are shown in Fig. 12. For both materials, the FIR limits of $\sigma_1(\omega)$ are in fair agreement with the measured

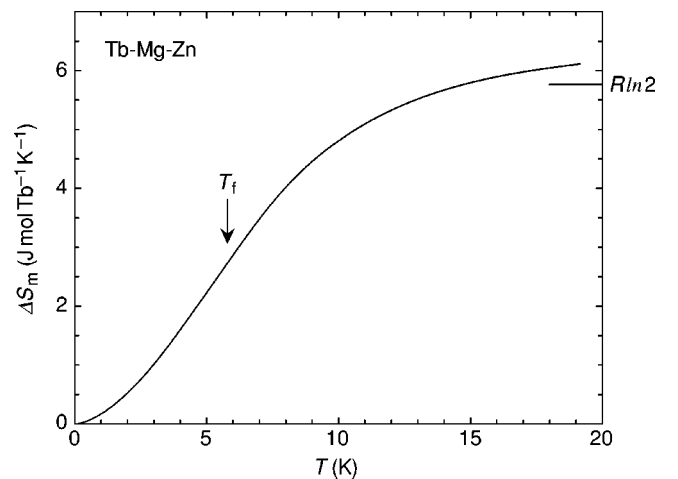


FIG. 10. The magnetic entropy ΔS_m of icosahedral Tb-Mg-Zn as a function of temperature T .

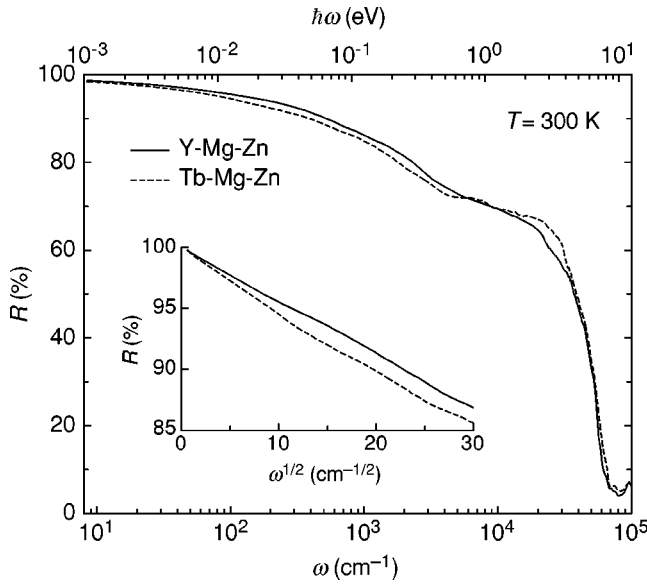


FIG. 11. Room-temperature optical reflectivity $R(\omega)$ of Y-Mg-Zn and Tb-Mg-Zn between 16 and $9.7 \times 10^4 \text{ cm}^{-1}$. Inset: R vs $\omega^{1/2}$ in the FIR spectral range for both materials.

electrical conductivities σ .⁷ This is illustrated in the inset of Fig. 12, which displays $\sigma_1(\omega)$ in the FIR spectral range.

Both the $R(\omega)$ and $\sigma_1(\omega)$ spectra reveal a number of features that have previously been identified for various other quasicrystalline systems. First, we clearly recognize the metallic behavior, indicated by a sharp plasma edge in $R(\omega)$ with an onset at approximately $6.5 \times 10^4 \text{ cm}^{-1}$ and the reflectivity $R(\omega)$ tending towards 100% for $\omega \rightarrow 0$. In the optical conductivity $\sigma_1(\omega)$ spectra, the metallic behavior manifests itself by the (Drude) spectral weight, i.e.,

$$\int_0^{\omega_0} \sigma_1(\omega) d\omega \quad (15)$$

at frequencies below $\omega_0 \sim 10^3 \text{ cm}^{-1}$ (see also inset of Fig. 12). Second, the reflectivity $R(\omega)$ spectra contain the above-mentioned typical broad shoulder between 8×10^3 and $2 \times 10^4 \text{ cm}^{-1}$ leading to an absorption peak at approximately $6 \times 10^3 \text{ cm}^{-1}$ in $\sigma_1(\omega)$, which overlaps with the Drude spectral weight and is ascribed to electronic excitation across a pseudogap. Due to the high dc electrical conductivity of the icosahedral Y-Mg-Zn and Tb-Mg-Zn quasicrystals, this absorption is less pronounced and appears at somewhat lower frequencies than for the icosahedral Al-Mn-Pd and Al-Re-Pd phases with lower conductivities (see, e.g., Fig. 13 in Ref. 38).^{17,32}

For Tb-Mg-Zn, two additional broad contributions may be identified at approximately 350 and 1000 cm^{-1} in the optical conductivity $\sigma_1(\omega)$ below the pseudogap absorption. The feature at 1000 cm^{-1} has previously been found in the $\sigma_1(\omega)$ spectra of icosahedral Al-Re-Pd.¹⁷ Contrary to an earlier interpretation in terms of a mobility gap feature,^{36,37} we suggested a distribution of bound states as an origin of this broad contribution in $\sigma_1(\omega)$ in Ref. 17. The FIR absorption at approximately 350 cm^{-1} in the $\sigma_1(\omega)$ spectra of Tb-Mg-Zn can be ascribed to optically active phonon modes. In fact, a peak near 240 cm^{-1} has been observed in the optical conductivity spectra of icosahedral quasicrystals and was as-

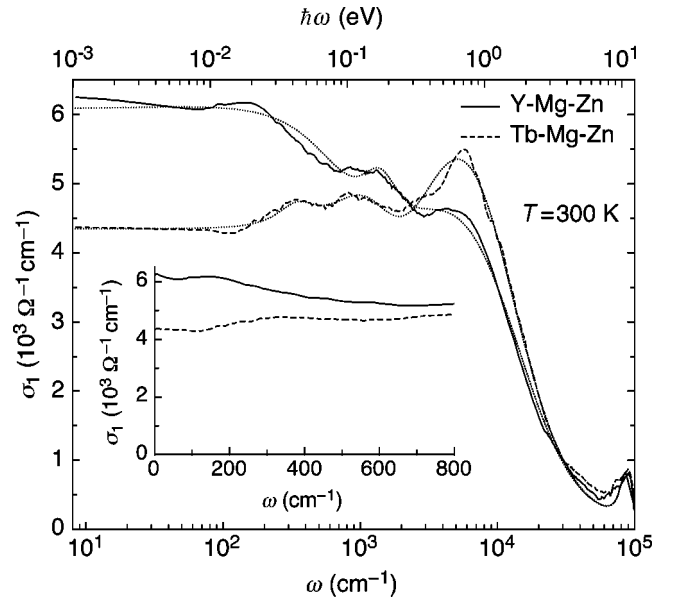


FIG. 12. Real part $\sigma_1(\omega)$ of the complex optical conductivity $\sigma(\omega)$ of Y-Mg-Zn and Tb-Mg-Zn at 300 K. The dotted lines indicate the fits of Eq. (16) to the σ_1 data. The inset shows $\sigma_1(\omega)$ in the FIR spectral range.

sociated with a phonon mode.^{17,32} Similar features in the spectral range extending from the midinfrared to the FIR can be also recognized in the Y-Mg-Zn compound. Despite the, in comparison with Tb-Mg-Zn, larger Drude spectral weight, an absorption and a broad shoulder at about 1000 and 200 cm^{-1} , respectively, may still be identified in $\sigma_1(\omega)$ of Y-Mg-Zn.

A phenomenological approach, based on the classical dispersion theory of Drude and Lorentz,⁴⁰ allows for a separation of the various components contributing to the dynamics of the charge excitation spectrum. For both quasicrystalline alloys, we assumed that $\sigma_1(\omega)$ can be described by a Drude term for the free charge carriers and several noninteracting Lorentz harmonic oscillators describing a phononlike excitation and a bound-state absorption below the pseudogap in the frequency range $\omega < 1.6 \times 10^3 \text{ cm}^{-1}$, a pseudogap-like absorption at $6 \times 10^3 \text{ cm}^{-1}$ and a high-frequency interband absorption. We model the dielectric function $\varepsilon(\omega)$ with

$$\varepsilon(\omega) = \varepsilon_\infty - \frac{\tilde{\omega}_p^2}{\omega(\omega + i\Gamma_D)} + \sum_{i=1}^4 \frac{\omega_i^2}{(\omega_i^0)^2 - \omega^2 - i\gamma_i\omega}, \quad (16)$$

where ε_∞ is the high-frequency dielectric constant; $\tilde{\omega}_p$ is the effective plasma frequency associated with the free charge carriers and Γ_D is the relaxation rate of the Drude term; ω_i^0 are the resonance frequencies, γ_i are the dampings, and ω_i are the mode strengths of the phonon, the bound state, the pseudogap and the interband harmonic oscillators, respectively. Fitting our $\sigma_1(\omega)$ data using Eq. (16) adequately reproduces the major features of the charge excitation spectrum (see Fig. 12). The values of the fitting parameters are given in Table I. We note that the values of the effective plasma frequencies $\tilde{\omega}_p$ are the largest, and the values of the pseudogap resonance frequencies ω_3^0 are the smallest ever

TABLE I. Parameters of the fits of Eq. (16) to the optical conductivity $\sigma_1(\omega)$ data of Y-Mg-Zn and Tb-Mg-Zn (see text).

Mode		Y-Mg-Zn	Tb-Mg-Zn
High-frequency dielectric response	ϵ_∞	1	1
Drude	$\tilde{\omega}_p, \text{cm}^{-1}$	1.95×10^4	1.69×10^4
	Γ_D, cm^{-1}	1.05×10^3	1.06×10^3
Phonon	$\omega_1^0, \text{cm}^{-1}$	2.26×10^2	3.47×10^2
	γ_1, cm^{-1}	1.86×10^3	2.82×10^2
	ω_1, cm^{-1}	2.10×10^3	2.34×10^3
Bound state	$\omega_2^0, \text{cm}^{-1}$	1.40×10^3	1.13×10^3
	γ_2, cm^{-1}	1.29×10^3	1.77×10^3
	ω_2, cm^{-1}	9.11×10^3	1.33×10^4
Pseudogap	$\omega_3^0, \text{cm}^{-1}$	5.08×10^3	5.73×10^3
	γ_3, cm^{-1}	1.58×10^4	1.44×10^4
	ω_3, cm^{-1}	6.30×10^4	6.53×10^4
Interband	$\omega_4^0, \text{cm}^{-1}$	8.55×10^4	8.55×10^4
	γ_4, cm^{-1}	2.00×10^4	2.00×10^4
	ω_4, cm^{-1}	2.82×10^4	2.82×10^4

reported for a quasiperiodically structured material.^{17,32,36–38} This observation is quite consistent with the previously recognized trends of the $\tilde{\omega}_p$ and ω_3^0 variations, which seem to be governed by the conducting character of a quasicrystalline phase.³⁸

An estimate of the spectral weight may be obtained by applying the conductivity sum rule to the $\sigma_1(\omega)$ spectrum

$$\int_0^\infty \sigma_1(\omega) d\omega = \frac{\omega_p^2}{8}, \quad (17)$$

with

$$\omega_p^2 = \frac{4\pi n_e e^2}{m^*}, \quad (18)$$

where n_e is the density of the charge carriers and m^* is their effective mass. Integrating the optical conductivity $\sigma_1(\omega)$ after having subtracted the contributions to $\sigma_1(\omega)$ from the high-frequency electronic interband transitions, the bound state and the phonon mode leads to $\omega_p = 6.59 \times 10^4$ and $6.73 \times 10^4 \text{ cm}^{-1}$ for Y-Mg-Zn and Tb-Mg-Zn, respectively. Assuming that the effective mass m^* is equal to the free-electron mass m , these plasma frequency values correspond to charge-carrier densities n_e of $4.85 \times 10^{22} \text{ cm}^{-3}$ for Y-Mg-Zn and $5.10 \times 10^{22} \text{ cm}^{-3}$ for Tb-Mg-Zn. We reiterate that these values reflect the density of *all* the charge carriers contributing to the complete charge excitation spectrum and are associated with the total spectral weight of the optical conductivity.

The concentration n_i and effective mass m^* of the *itinerant* charge carriers may be estimated from a comparison of the coefficient γ_{el} of the electronic specific heat and the effective plasma frequency $\tilde{\omega}_p$. For Y-Mg-Zn, assuming that the linear term γT in the low-temperature specific heat $C_p(T)$ is entirely due to the density of electronic states at the

Fermi energy E_F (see Sec. III B), leads to an itinerant charge carrier density $n_i = 7.62 \times 10^{21} \text{ cm}^{-3}$, or 0.13 charge carriers per atom, and an effective mass $m^* \approx 1.8m$.

IV. SUMMARY

For icosahedral Y-Mg-Zn, the temperature dependence of the electrical conductivity $\sigma(T)$ between 14 and 150 K and the magnetic field dependence of the magnetoconductivity $\delta\sigma(H)$ in magnetic fields of up to 70 kOe and in the temperature range between 4 and 30 K can be well described quantitatively by considering weak localization in the presence of spin-orbit scattering of moderate strength. The temperature variation of the inelastic scattering rate $\tau_i^{-1}(T) \propto T^3$ that can be inferred from our electrical conductivity $\sigma(T)$ and magnetoconductivity $\delta\sigma(H)$ data is consistent with theoretical expectations for electron-phonon scattering in pure metals, which is quite surprising in view of the quasiperiodic structure of icosahedral Y-Mg-Zn. The temperature variation of the conductivity $\sigma(T)$ between 1.8 and 14 K indicates that another mechanism, most likely Coulomb interactions among itinerant electrons, contributes albeit weakly to $\sigma(T)$ in this temperature range.

Below 4 K, the specific heat $C_p(T)$ of icosahedral Y-Mg-Zn can be well described as the sum of a linear- and a cubic-in-temperature terms, i.e., assuming that $C_p(T)$ is due to electronic and lattice excitations. The coefficient γ of the linear term γT in the specific heat $C_p(T)$ is close to the γ value of zinc, thus indicating no significant reduction in the density of electronic states at E_F . For Tb-Mg-Zn, the temperature variation of the specific heat $C_p(T)$ is indicative of a spin-glass-type freezing of Tb moments and of a crystal-field splitting of the Tb $J=6$ Hund's rule ground state.

The optical conductivity $\sigma_1(\omega)$ spectra of icosahedral Y-Mg-Zn and Tb-Mg-Zn reveal a number of common features. At low frequencies, $\sigma_1(\omega)$ is dominated by a Drude contribution with the effective plasma frequencies $\tilde{\omega}_p$ associated with the free charge carriers of 1.95×10^4 and $1.69 \times 10^4 \text{ cm}^{-1}$ for Y-Mg-Zn and Tb-Mg-Zn, respectively. The relaxation rate Γ_D of the free charge carriers is only about $1 \times 10^3 \text{ cm}^{-1}$ for both icosahedral phases. This value is distinctly smaller than the Γ_D values previously deduced from the optical conductivity $\sigma_1(\omega)$ spectra of Al-based quasicrystals with FCI structures^{17,32,36,37} and is even smaller than typical relaxation rates in amorphous metals.⁴¹ This is a further manifestation of the enhanced *metallicity* of the Y- and Tb-based single-grain icosahedral quasicrystals. In the near infrared and visible spectral range, the most prominent feature in the $\sigma_1(\omega)$ spectra of these quasicrystalline materials is an absorption centered at approximately $6 \times 10^3 \text{ cm}^{-1}$, which is attributed to excitations across a pseudogap in the electronic excitation spectrum. Due to the rather high electrical conductivity of icosahedral Y-Mg-Zn and Tb-Mg-Zn in the low-frequency limit, this absorption occurs at distinctly lower frequency than for the FCI Al-Mn-Pd and Al-Re-Pd quasicrystals. For icosahedral Y-Mg-Zn, a density n_i of the free charge carriers of $7.62 \times 10^{21} \text{ cm}^{-3}$ and a mass enhancement $m^*/m \approx 1.8$ may be inferred from a direct comparison of the effective plasma frequency $\tilde{\omega}_p$ and the coefficient γ of the linear term γT in the low-temperature specific heat $C_p(T)$.

ACKNOWLEDGMENTS

M.A.C. would like to thank the Texas Center for Superconductivity at the University of Houston for its hospitality during part of this work. L.D. would like to thank P. Wachter

for his generous support in providing infrastructure related with these experiments. This work was in part financially supported by the Schweizerische Nationalfonds zur Förderung der wissenschaftlichen Forschung.

- *Present address: Texas Center for Superconductivity, University of Houston, Houston, TX 77204.
- †Present address: Max-Planck-Institut für chemische Physik fester Stoffe, Nöthnitzerstrasse 48, 01187 Dresden, Germany.
- ¹Z. Luo, S. Zhang, Y. Tang, and D. Zhao, *Scr. Metall.* **28**, 1513 (1993).
- ²E. M. Padezhnova, E. V. Mel'nik, R. A. Miliyevskiy, T. V. Dobatkina, and V. V. Kinzhbalo, *Russ. Metall.* **3**, 1985 (1982).
- ³A. P. Tsai, A. Niikura, A. Inoue, T. Masumoto, Y. Nishida, K. Tsuda, and M. Tanaka, *Philos. Mag. Lett.* **70**, 169 (1994).
- ⁴I. R. Fisher, Z. Islam, A. F. Panchula, K. O. Cheon, M. J. Kramer, P. C. Canfield, and A. I. Goldman, *Philos. Mag. B* **77**, 1601 (1998).
- ⁵A. Langsdorf, F. Ritter, and W. Assmus, *Philos. Mag. Lett.* **75**, 381 (1997).
- ⁶M. J. Kramer, P. C. Canfield, I. R. Fisher, S. Kycia, and A. I. Goldman, in *Proceedings of the 7th International Conference on Quasicrystals, Stuttgart, Germany, 1999*, edited by F. Gähler, P. Kramer, H.-R. Trebin, and K. Urban [*Mater. Sci. Eng. A* (to be published)].
- ⁷I. R. Fisher, K. O. Cheon, A. F. Panchula, P. C. Canfield, M. A. Chernikov, H. R. Ott, and K. Dennis, *Phys. Rev. B* **59**, 308 (1999).
- ⁸A. Kawabata, *J. Phys. Soc. Jpn.* **49**, 628 (1980).
- ⁹H. Fukuyama and K. Hoshino, *J. Phys. Soc. Jpn.* **50**, 2131 (1981).
- ¹⁰L. P. Gor'kov, A. I. Larkin, and D. E. Khmel'nitskii, *Pis'ma Zh. Éksp. Teor. Fiz.* **30**, 248 (1979) [*JETP Lett.* **30**, 228 (1979)].
- ¹¹S. Koshino, *Prog. Theor. Phys.* **24**, 1049 (1960).
- ¹²Yu. Kagan and A. P. Zhernov, *Zh. Éksp. Teor. Fiz.* **50**, 1107 (1966) [*Sov. Phys. JETP* **23**, 737 (1966)].
- ¹³A. Schmid, *Z. Phys.* **271**, 251 (1973).
- ¹⁴B. L. Al'tshuler and A. G. Aronov, *Pis'ma Zh. Éksp. Teor. Fiz.* **30**, 514 (1979) [*JETP Lett.* **30**, 482 (1979)].
- ¹⁵T. Klein, H. Rakoto, C. Berger, G. Fourcaudot, and F. Cyrot-Lackmann, *Phys. Rev. B* **45**, 2046 (1992).
- ¹⁶M. A. Chernikov, A. Bernasconi, C. Beeli, and H. R. Ott, *Europhys. Lett.* **21**, 767 (1993).
- ¹⁷A. D. Bianchi, F. Bommeli, M. A. Chernikov, U. Gubler, L. Degiorgi, and H. R. Ott, *Phys. Rev. B* **55**, 5730 (1997).
- ¹⁸R. Kondo, T. Hashimoto, K. Edagawa, S. Takeuchi, T. Takeuchi, and U. Mizutani, *J. Phys. Soc. Jpn.* **66**, 1097 (1997).
- ¹⁹P. Lindqvist and Ö. Rapp, *J. Phys. F: Met. Phys.* **18**, 1979 (1988).
- ²⁰D. V. Baxter, R. Richter, M. L. Trudeau, R. W. Cochrane, and J. O. Ström-Olsen, *J. Phys. (France)* **50**, 1673 (1989).
- ²¹P. Lindqvist, C. Berger, T. Klein, P. Lanco, F. Cyrot-Lackmann, and Y. Calvayrac, *Phys. Rev. B* **48**, 630 (1993).
- ²²Y. Hattori, A. Niikura, A. P. Tsai, A. Inoue, T. Masumoto, K. Fukamichi, H. Aruga-Katori, and T. Goto, *J. Phys.: Condens. Matter* **7**, 2313 (1995).
- ²³N. Vernier, G. Bellessa, B. Perrin, A. Zarembowitch, and M. de Boissieu, *Europhys. Lett.* **22**, 187 (1993).
- ²⁴M. A. Chernikov, A. Bianchi, and H. R. Ott, *Phys. Rev. B* **51**, 153 (1995).
- ²⁵M. A. Chernikov, A. D. Bianchi, E. Felder, U. Gubler, and H. R. Ott, *Europhys. Lett.* **35**, 431 (1996).
- ²⁶P. W. Anderson, B. I. Halperin, and C. M. Varma, *Philos. Mag.* **25**, 1 (1972).
- ²⁷W. A. Phillips, *J. Low Temp. Phys.* **7**, 351 (1972).
- ²⁸R. O. Pohl, in *Amorphous Solids: Low-Temperature Properties*, edited by W. A. Phillips, *Topics in Current Physics Vol 24* (Springer-Verlag, Berlin, 1981), Chap. 3, p. 27.
- ²⁹K. Giannò, A. Sologubenko, M. A. Chernikov, H. R. Ott, I. R. Fisher, and P. C. Canfield, in *Proceedings of the 7th International Conference on Quasicrystals* (Ref. 6).
- ³⁰B. Lüthi (unpublished).
- ³¹M. A. Chernikov, A. Bernasconi, C. Beeli, A. Schilling, and H. R. Ott, *Phys. Rev. B* **48**, 3058 (1993).
- ³²L. Degiorgi, M. A. Chernikov, C. Beeli, and H. R. Ott, *Solid State Commun.* **87**, 721 (1993).
- ³³J. O. Thomson and J. R. Thomson, *J. Phys. F: Met. Phys.* **11**, 247 (1981).
- ³⁴R. Caudron, P. Costa, J. C. Lasjaunias, and B. Levesque, *J. Phys. F: Met. Phys.* **11**, 451 (1981).
- ³⁵R. J. Trainor, Jr. and D. C. McCollum, *Phys. Rev. B* **9**, 2145 (1974).
- ³⁶C. C. Homes, T. Timusk, X. Wu, Z. Altounian, A. Sahnoune, and J. O. Ström-Olsen, *Phys. Rev. Lett.* **67**, 2694 (1991).
- ³⁷D. N. Basov, F. S. Pierce, P. Volkov, S. J. Poon, and T. Timusk, *Phys. Rev. Lett.* **73**, 1865 (1994).
- ³⁸A. D. Bianchi, F. Bommeli, E. Felder, M. Kenzelmann, M. A. Chernikov, L. Degiorgi, H. R. Ott, and K. Edagawa, *Phys. Rev. B* **58**, 3046 (1998).
- ³⁹S. E. Burkov, T. Timusk, and N. W. Ashcroft, *J. Phys.: Condens. Matter* **4**, 9447 (1992).
- ⁴⁰F. Wooten, *Optical Properties of Solids* (Academic, New York, 1972).
- ⁴¹S. W. McKnight and A. K. Ibrahim, *J. Non-Cryst. Solids* **61&62**, 1301 (1984).